

1 **BIRDMAN: A Bayesian differential abundance framework that enables** 2 **robust inference of host-microbe associations**

3
4 Gibraan Rahman^{1,2}, James T. Morton³, Cameron Martino^{1,2}, Gregory D. Sepich-Poore⁴, Celeste
5 Allaband¹, Caitlin Guccione^{1,2,5}, Yang Chen^{1,6,7}, Daniel Hakim^{1,2}, Mehrbod Estaki⁸, Rob Knight^{1,9}

6
7 ¹Department of Pediatrics, University of California San Diego, La Jolla, CA, USA

8 ²Bioinformatics and Systems Biology Program, University of California San Diego, La Jolla, CA,
9 USA

10 ³Biostatistics & Bioinformatics Branch, Eunice Kennedy Shriver National Institute of Child Health
11 and Human Development, National Institutes of Health, Bethesda, MD, USA

12 ⁴Micronoma, San Diego, CA, USA

13 ⁵Division of Biomedical Informatics, Department of Medicine, University of California San Diego,
14 La Jolla, CA

15 ⁶Department of Dermatology, University of California San Diego, La Jolla, CA, USA

16 ⁷Biomedical Sciences Graduate Program, University of California San Diego, La Jolla, CA

17 ⁸Department of Physiology & Pharmacology, University of Calgary, Calgary, Canada

18 ⁹Department of Computer Science and Engineering, University of California, San Diego, La
19 Jolla, California, USA

20 **Abstract**

21 Quantifying the differential abundance (DA) of specific taxa among experimental groups in
22 microbiome studies is challenging due to data characteristics (e.g., compositionality, sparsity)
23 and specific study designs (e.g., repeated measures, meta-analysis, cross-over). Here we
24 present BIRDMAN (**B**ayesian **I**nferral **R**egression for **D**ifferential **M**icrobiome **A**nalysis), a
25 flexible DA method that can account for microbiome data characteristics and diverse
26 experimental designs. Simulations show that BIRDMAN models are robust to uneven
27 sequencing depth and provide a >20-fold improvement in statistical power over existing
28 methods. We then use BIRDMAN to identify antibiotic-mediated perturbations undetected by
29 other DA methods due to subject-level heterogeneity. Finally, we demonstrate how BIRDMAN
30 can construct state-of-the-art cancer-type classifiers using The Cancer Genome Atlas (TCGA)
31 dataset, with substantial accuracy improvements over random forests and existing DA tools
32 across multiple sequencing centers. Collectively, BIRDMAN extracts more informative biological
33 signals while accounting for study-specific experimental conditions than existing approaches.

34

35 Main

36 Advances in sequencing technology and computational methods have enabled researchers to
37 experimentally characterize microbiomes across wide ranges of biological conditions, including
38 psychiatric diseases^{1,2}, cancer^{3,4}, and COVID-19^{5,6}. However, as the understanding of microbial
39 effects on human health and disease has increased, the experimental questions, hypotheses,
40 and concomitant statistics have grown in complexity, with study designs now commonly
41 involving longitudinal analyses⁷⁻⁹, experimental interventions¹⁰⁻¹², and meta-analyses⁷. Although
42 such approaches can provide mechanistic insights into the microbiome's effect(s) on the host,
43 their conclusions are often limited by the ability to perform valid statistical analyses that are
44 sufficiently flexible to account for the added experimental complexity.

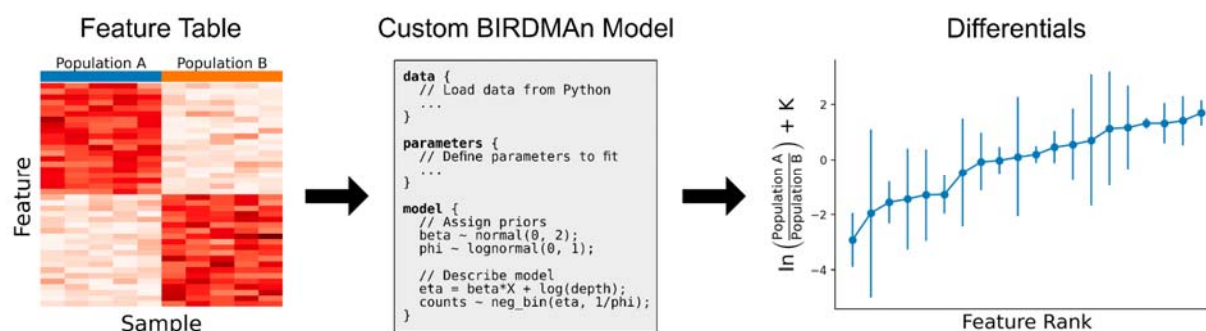
45
46 One common but critical challenge in these contexts is when population-level heterogeneity
47 (such as subject-to-subject variation) is confounded by technical variability. For example,
48 samples originating from the same sequencing center will tend to be more similar to each other
49 than those sequenced from different centers¹³. The confounding factors that may explain these
50 differences make it difficult to determine consistent microbial biomarkers associated with
51 biological variables or conditions of interest⁸—an effect compounded by other microbiome data
52 difficulties, such as high sparsity, high-dimensionality, and compositionality. Moreover, statistical
53 tools that can properly assess and account for strong structural effects while still indicating
54 which microbes truly vary between biological conditions are limited to date¹⁵.

55
56 Making matters more difficult, disagreement exists about how to benchmark differential
57 abundance (DA) tools and methods. Previous efforts have commonly focused on comparing the
58 results of hypothesis testing while accounting for the multiplicity of features through false-
59 discovery-rate (FDR) correction¹⁵⁻¹⁷. Studies have demonstrated that tools designed for
60 differential abundance often report contradictory results with different microbial abundances
61 among biologically distinct sampling groups¹⁹.

62
63 Addressing these challenges requires a more robust statistical framework for benchmarking
64 differential abundance methods and would benefit from flexible DA modeling approaches. Thus,
65 we developed BIRDMan (**B**ayesian **I**nferral **R**egression for **D**ifferential **M**icrobiome **A**nalysis),
66 a flexible computational framework for hierarchical Bayesian modeling of microbiome data that
67 simultaneously accounts for its high sparsity, high-dimensionality, and compositionality.

68
69 The Bayesian approach to statistical modeling provides unique advantages compared to
70 frequentist solutions, such as the inclusion of prior information, uncertainty estimation of
71 parameters, native hierarchical modeling, and edge case smoothing (e.g., estimating log fold
72 changes when a feature is only present in one group). Implemented within the Stan
73 programming language (commonly used for designing probabilistic models), BIRDMan flexibly
74 enables parameter estimation of all biological variables and non-biological covariates. These
75 advantages allow us to demonstrate how explicitly modeling population-level effects in
76 probabilistic BIRDMan models increases the amount of true biological signal recovered
77 compared to existing tools on both simulated and real-world datasets. Moreover, the BIRDMan

78 workflow significantly lowers the barrier of entry for differential abundance methods
79 development and implementation. Additionally, to address reproducibility issues of prior DA tool
80 benchmarking, we present a novel approach that employs techniques from compositional data
81 analysis, making the comparison of tools more interpretable and statistically valid.
82



83
84 **Fig 1:** Overview of BIRDMan workflow for customizable differential abundance analysis. A table
85 of counts by features is modeled using Bayesian probabilistic programming, resulting in credible
86 intervals of the estimated parameter posterior distributions. The statistical model can be
87 customized using the Stan probabilistic programming language and fit using the BIRDMan
88 Python interface.

89 Results

90 BIRDMan is implemented as a Python interface to the Stan probabilistic programming
91 language, which utilizes Hamiltonian Monte Carlo sampling, one of the state-of-the-art
92 approaches for Bayesian uncertainty estimation²⁰. Users can employ pre-configured model
93 designs or flexibly customize inputs to account for their specific experimental design and
94 biological questions; BIRDMan then fits and processes these models (Fig 1). The results of
95 these analyses are the posterior distributions of the defined parameters of interest, such as log-
96 fold changes and their uncertainty given the data (see Methods).

97
98 To showcase the statistical properties of BIRDMan models, we first leverage simulations to
99 evaluate the accuracy of estimating differential uncertainty in the context of realistic biological
100 scenarios. Then, we apply BIRDMan models on real-world data, demonstrating superiority for
101 resolving subject-level heterogeneity in an antibiotics experiment, as well as alleviating
102 sequencing center-specific effects in a cancer genomics dataset, each while capturing
103 biologically-informative signals.

104 Simulations demonstrate BIRDMan model accuracy and precision

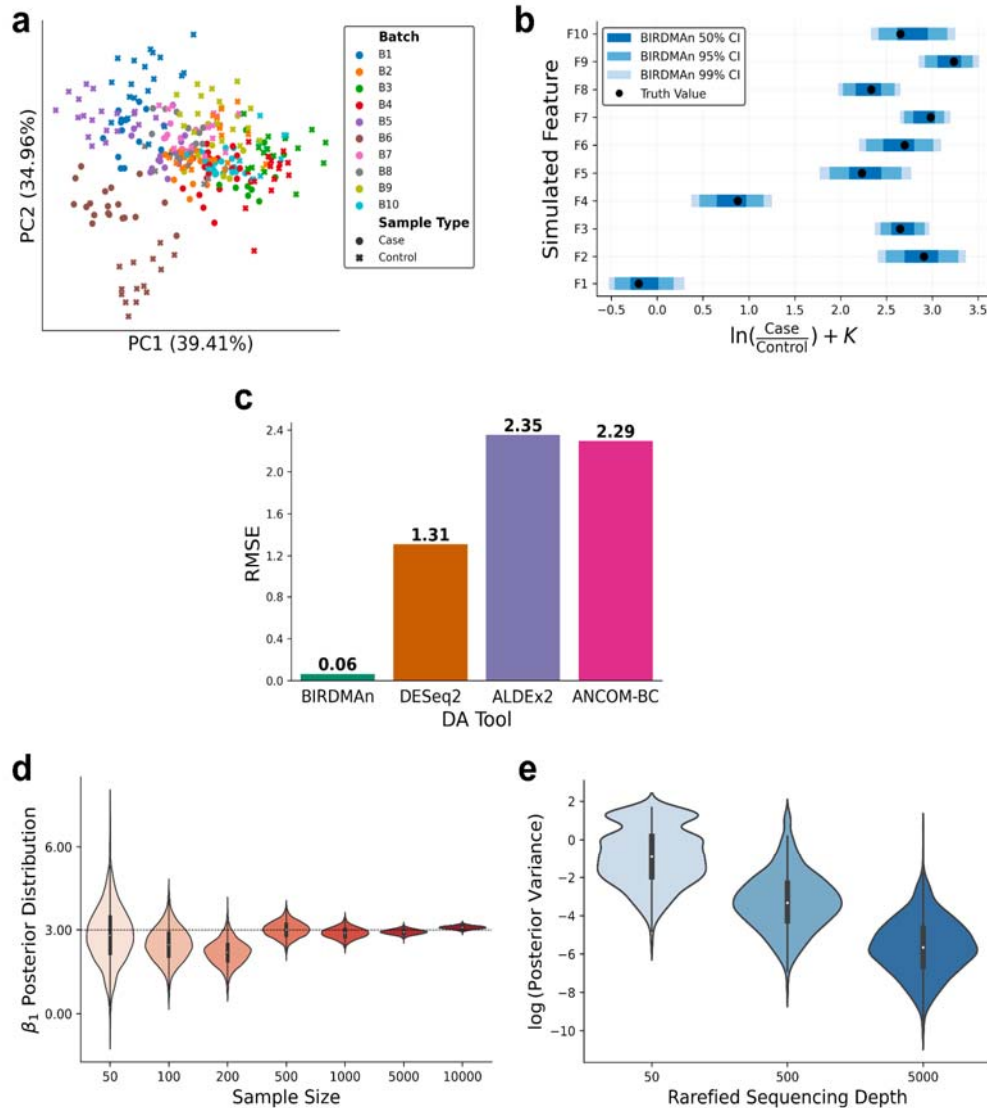
105 A common difficulty in benchmarking differential abundance methods is the lack of ground truth.
106 We typically do not know which microbial taxa are truly increasing or decreasing across
107 experimental conditions. To gain insights into the robustness of BIRDMan models, we
108 performed a data-driven simulation of a case-control microbiome dataset with one binary
109 covariate, large batch effects (10 features, 10 batches, and 300 samples), data overdispersion,

110 and known differentials associated with case status (see Methods) (Fig 2a). We then used
111 BIRDMAN to estimate the model parameters for each feature and compared the Bayesian
112 posterior estimates with the true value, finding that BIRDMAN models recovered the ground
113 truth differentials with high accuracy and precision (Fig 2b) while outperforming other tools in
114 terms of root mean square error (RMSE) (Fig 2c). This highlights how BIRDMAN model
115 customization permits more accurate estimations of differentials.

116

117 One advantage of Bayesian models is that they can leverage posterior estimates to summarize
118 the uncertainty of these differentials, taking into account the sample size and the sequencing
119 depth. As expected, we show that when BIRDMAN models are fitted on larger sample sizes, the
120 uncertainty decreases, highlighting how incorporating more data, and avoiding rarefaction,
121 enables a more accurate estimation of the differentials (Fig 2d). Furthermore, we show that
122 decreasing the sequencing depth also increases the uncertainty, highlighting how rarefaction
123 could degrade parameter estimates' precisions in BIRDMAN models (Fig 2e). Since BIRDMAN
124 can handle variable sequencing depths, there is no need to perform rarefaction before model
125 fitting, which is desirable when analyzing microbiome datasets²¹.

126



127
128

129 **Fig 2:** (a) Robust Aitchison principal components plot of the simulated data, showing the large
130 separation by batch effect. Simulations of 10 batches (B1 to B10) of microbiome results, each
131 containing 10 features (F1 to F10), where each feature has a true differential abundance
132 between cases and controls that is the same for each batch, and also a random per batch bias.
133 (b) Recovery of the true simulated log ratio between cases and controls for each feature (black
134 dots), with credible intervals on average centered on the true log ratio (blue bars). (c) Superior
135 performance of BIRDMAN over other differential abundance methods in minimizing the RMSE of
136 the difference between the estimated mean posterior log ratio between cases and controls,
137 revealing a >20-fold improvement in RMSE over the nearest competitor, DESeq2. (d) Estimated
138 distributions of log-fold changes from Bayesian analysis tighten as the number of samples
139 increases. Dashed line represents the true simulated value for each simulation. (e) Rarefaction
140 simulation performed using multinomial count generative models (1000 features) at three

141 *different sequencing depths shows that the variance of the posterior distribution decreases as*
142 *depth increases.*

143 BIRDMAN models capture biological signals missed by other methods 144 during dual-course longitudinal antibiotics

145
146 Another challenge for DA methods is to compare multiple samples from the same subject
147 longitudinally (repeated measures) since concomitant host-specific variation can obscure
148 phenotypically-associated microbial changes. Methods designed for longitudinal data²²⁻²⁶
149 cannot easily account for modeling perturbations and struggle with scaling to high dimensions.
150 To demonstrate the use of BIRDMAN on repeated measure study designs, we evaluated a
151 published longitudinal study of two courses of the antibiotic ciprofloxacin (Cp) (3 subjects, 7
152 timepoints)²⁷. Notably, this study originally concluded that inter-subject variability drove the
153 response to antibiotics by examining beta-diversities, which do not account for auto-correlation
154 effects of repeated measures²⁸ (Fig 3a). Other studies have also highlighted the importance of
155 properly accounting for the microbial community composition prior to antibiotics when assessing
156 varying responses^{29,30}, which requires accurate temporal modeling.

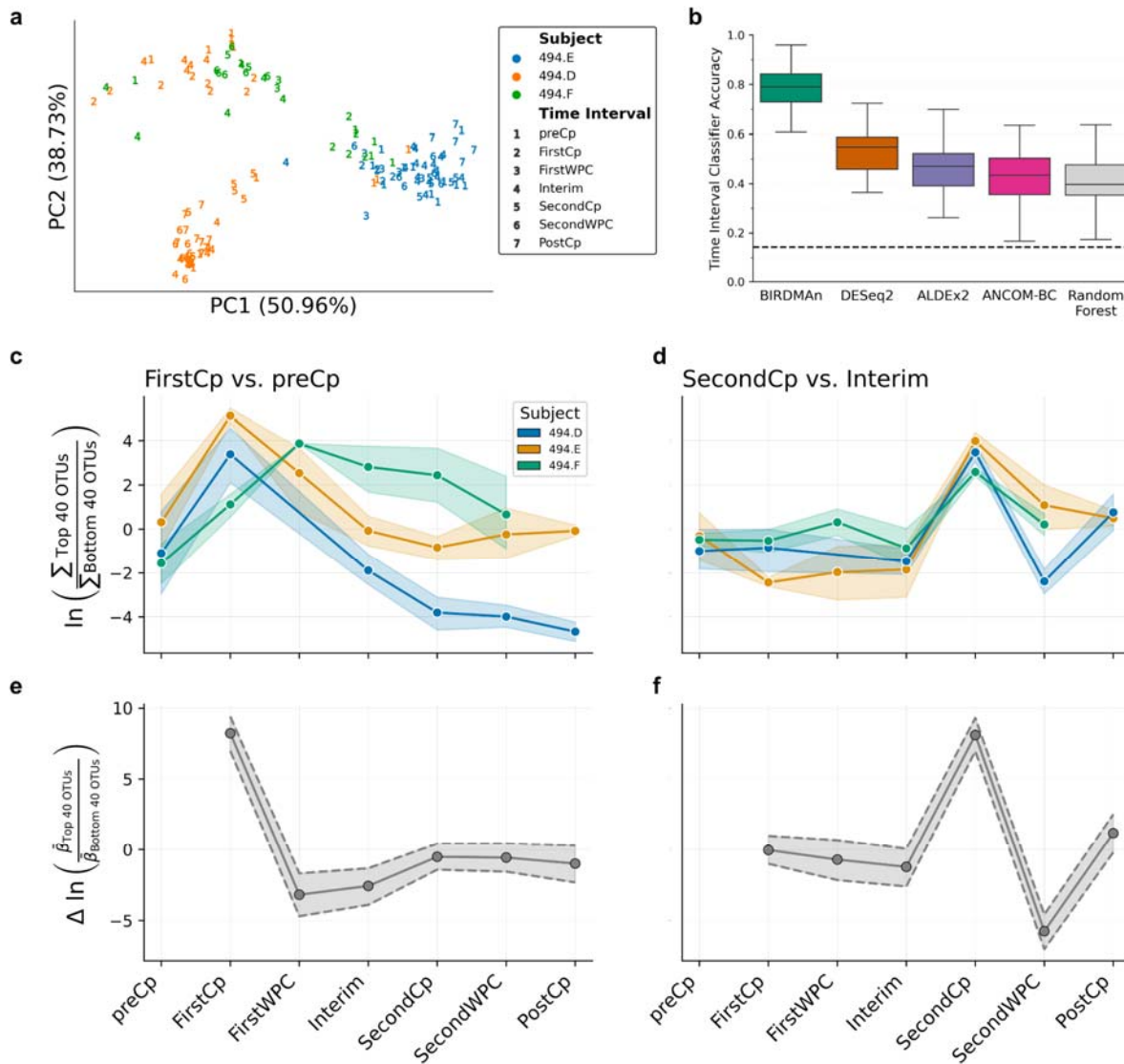
157
158 Given BIRDMAN's flexibility, we constructed a customized DA model that leverages Linear
159 Mixed Effects models, accounting for repeated measurements from subjects while computing
160 temporal differences (see Methods). This model design then enabled the exploration of common
161 microbial community changes associated with antibiotic perturbation, which the originally
162 published methods could not identify. With the computed log-fold changes over time (Supp Fig
163 1a), we investigated how consistent antibiotic induced shifts were across subjects. For each
164 temporal difference, we took the top and bottom 40 OTUs to calculate sample log-ratios, which
165 were used to predict antibiotics intake³¹. From these log-ratios, we observed strong, statistically
166 significant temporal shifts associated with each successive time interval (Supp Fig 1b).

167
168 To determine if existing tools could have identified these timepoint-specific perturbations, we
169 also developed a multinomial logistic regression classifier based on the BIRDMAN results to
170 predict the corresponding time interval. We then compared our prediction performances against
171 classifiers built using ALDEx2³², ANCOM-BC³³, and DESeq2³⁴ results on the same samples, as
172 well as a classifier built on the center log-ratio transformed table (see Methods). Remarkably,
173 BIRDMAN-informed classifiers were able to accurately differentiate between the different
174 treatment groups (accuracy > 0.65) (Supp Fig 1c) and showed substantially better prediction
175 accuracy compared to all other methods (Fig 3b). We also verified that this superior
176 performance held across varying numbers of OTUs used in log-ratio calculation (Supp Fig 1d).
177 Ultimately, these findings show how BIRDMAN can identify clear-cut biological changes that
178 were missed or obscured by other approaches, highlighting its ability to confirm expected
179 biological hypotheses.

180
181 We used the sample log-ratios associated with the First and Second Cp applications and plotted
182 the dynamics over time (Fig 3c, d). Accordingly, we plotted the corresponding derivative log-fold

183 changes computed from BIRDMAn (Fig 3e, f) and see that our trajectories match between the
184 sample log-ratios and the estimated log-fold changes, indicating that our model was able to
185 successfully capture the overall signal independent of subject.

186
187 The antibiotic used in the original work, Cp, is known to primarily target (though not exclusively)
188 gram negative bacteria^{35,36}. We thus hypothesized that the differential abundance results should
189 reflect the longitudinal dynamics of gram negative bacterial abundance. In the top and bottom
190 40 most changed taxa after FirstCp, 17.5% of the numerator taxa were gram negative, whereas
191 27.5% of the denominator were gram negative (Supp Fig 2e). Given the Cp antibiotic
192 mechanism, it is likely that gram negative taxa in the denominator decreased which caused the
193 increased log-ratio^{37,38} (Figure 2c). We see that there is a sharp decrease in this log-ratio at
194 FirstWPC, which could be attributed to gut homeostasis^{37,38}. However, we see a weaker pattern
195 in the top/bottom 40 microbes after SecondCp, where 2.5% of the numerator taxa were gram
196 negative and 10% of the denominator taxa were gram negative. In contrast to the FirstCp, the
197 microbes most affected by SecondCp quickly returned to their original abundances.
198 Furthermore, we see that the microbes most altered by FirstCp were not affected by SecondCp.
199 Altogether this hints at newly acquired antimicrobial resistant genes after the application of
200 FirstCp.



201
 202 **Fig 3:** (a) Robust Aitchison principal components plot of full dataset shows samples cluster
 203 primarily by host subject. (b) Balanced accuracy of multinomial classification of time point by
 204 tool. Differential abundance classifiers were constructed using logistic regression with the log-
 205 ratios of the top 40 and bottom 40 OTUs associated with each timepoint as predictors.
 206 Repeated k-fold cross-validation was performed with 5 splits and 10 repeats. The mean
 207 classifier error is at least twice as great with all other differential abundance tools as with
 208 BIRDMan. Dashed line represents random guessing performance among the seven timepoints.
 209 (c, d) Dynamics of sample log-ratios of (c) first Cp course and (d) second Cp course colored by
 210 subject. (e, f) Dynamics of BIRDMan-estimated log-fold changes associated with (e) FirstCp
 211 effect with preCp as reference and (f) SecondCp effect with Interim as reference. Shaded
 212 intervals represent the 90% credible interval of the estimated posterior distributions.
 213

214 BIRDMAN models mitigate batch effects in cancer microbiome data

215 To investigate how generalizable BIRDMAN models are with respect to population
216 heterogeneity, we conducted a meta-analysis using cancer microbiome data derived from The
217 Cancer Genome Atlas (TCGA). This dataset is known to have large structural batch effects⁴,
218 where the samples were processed at multiple centers across North America, resulting in an
219 artificial separation of cancer microbiomes by sequencing center if not otherwise accounted for
220 (Fig 4a, Supp Fig 2a)^{4,39}. These effects can make it difficult to determine microbial biomarkers
221 associated with tumors rather than artifacts of technical variation, but correcting for this could
222 enable downstream host-microbial cancer analyses. We thus tested how well BIRDMAN models
223 could extract biological signals from this dataset while accounting for technical batch effects
224 modeled as random effects. We additionally modeled each microbial feature's abundance using
225 this approach to determine the specificity of these microbes for each cancer type (see Methods
226 and Code).

227
228 Since cancer types are known to have distinct microbiomes^{4,40}, we first confirmed that BIRDMAN
229 models could extract cancer type-specific differences despite the technical variation observed in
230 this study. From our log-ratio classification benchmarks, we observe that our custom BIRDMAN
231 model can detect a substantially stronger differential signature between the cancer types
232 compared to ALDEx2, ANCOM-BC, DESeq2, and Random Forests (Fig 4b; note the axis log-
233 scaling) after controlling for the batch effects due to the sequencing center (Supp Fig 2c).

234
235 To determine the generalizability of our results, we then constructed a leave-one-center-out
236 cross-validation benchmark using logistic regression on the BIRDMAN-computed log-ratios.
237 Four cancer types with at least three represented data submitting centers (head and neck
238 cancer [HNSC], bladder cancer [BLCA], thyroid cancer [THCA], and cervical cancer [CESC])
239 were included in this benchmark. The receiver operating characteristic (ROC) curves
240 demonstrated strong classification performance (Fig 4c), indicating that BIRDMAN captures
241 generalizable microbial signals across multiple sequencing centers. Generalizability can be a
242 major challenge in microbiome studies³, where classifiers become overfitted for individual
243 cohorts. We observe this with other DA tools (ALDEx2, DESeq2, ANCOM-BC) and even
244 Random Forests (Supp Fig 2d), where most tools struggle to achieve an area under the ROC
245 curves (AUROC) of >0.8. BIRDMAN is competitive with these tools, achieving an AUROC >0.9
246 in HNSC, BLCA, and CESC cancers while achieving the highest predictive accuracy in BLCA
247 and CESC cancers. The high classifier accuracy leaving out each individual center
248 demonstrates that no one center's data strongly affects the classifier accuracy, with the
249 exception of BI for THCA.

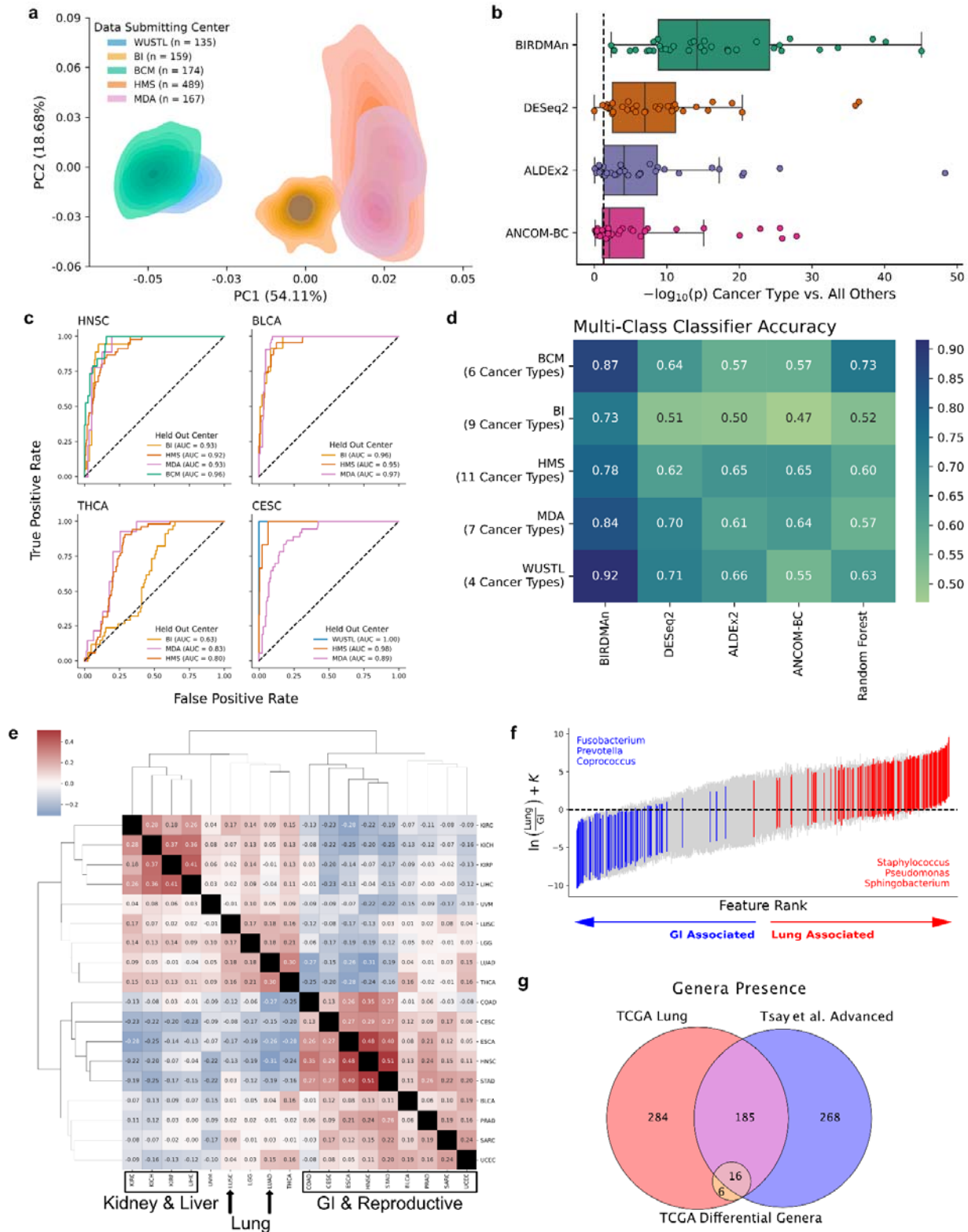
250
251 To investigate the heterogeneity across different cancer types, we next computed Kendall
252 correlations of BIRDMAN-estimated microbial log-fold changes across all pairs of cancer types.
253 This analysis revealed similarities among cancer types that we would expect, including strong
254 similarities between kidney cancer subtypes (KIRC, KICH, KIRP), lung cancer subtypes (LUAD,
255 LUSC), and gastrointestinal (GI) cancers (COAD, ESCA, HNSC, STAD). Additionally, the
256 BIRDMAN-informed data suggested some novel associations, such as the similarity between
257 kidney cancers and liver cancer (LIHC). When clustering the individual microbes' differentials

258 (Supp Fig 2b), we also observed that numerous GI-specific microbes differentiated GI cancers
259 from other cancer types.

260

261 When focusing on comparing GI cancers to lung cancers, we found that the resulting BIRDMAN
262 log-fold changes accurately reflected known biology surrounding the niches in which these
263 microbiomes are commonly found. Specifically, *Fusobacterium*⁴¹, *Prevotella*⁴², and *Coproccus*⁴³
264 are genera commonly found in the GI tract; conversely, *Pseudomonas*⁴⁴, *Staphylococcus*⁴⁵, and
265 *Sphingobacterium*⁴⁶ genera include opportunistic pathogens that are commonly found in lung
266 infections (Fig 4f). We cross-referenced our results against the Tsay *et al.* cohort that utilized
267 16S rRNA sequencing to investigate lung cancer. Out of the 469 genera in the TCGA lung
268 issues, we observed that 39% of these microbes were also observed in the Tsay *et al.* cohort,
269 despite known previous discordant findings comparing 16S rRNA sequencing and whole
270 genome sequencing^{47,48}. Furthermore, when we focus on the top 100 microbes that are
271 detected to be associated with lung cancer, 70% of the represented genera were observed in
272 both the TCGA and Tsay *et al.* datasets. Altogether, this shows how BIRDMAN models can
273 provide biologically-informative results while properly accounting for and mitigating strong
274 structural batch effects that currently confound other DA approaches.

275



276

277

278

279

Fig 4: (a) Whole-genome sequenced cancer microbiome data from TCGA shows strong batch effects by sequencing center (colored by center; see Supp Fig 2a for per cancer type plots). Samples are summarized by the 2D kernel density estimate for each center. (b) T-test p-values

280 *comparing log-ratios of each cancer type vs. all others within each center. Dashed line*
281 *represents $p=0.05$. All differential abundance methods show significant differences with log-*
282 *ratios to separate the microbes in each individual cancer type from those found in all other*
283 *cancer types, but BIRDMAN outperforms other methods in highlighting this difference. (c) ROC*
284 *curves for leave-one-center-out cross-validation for four cancer types where at least 3 centers*
285 *sequenced that cancer type (BRCA was not included as it was used as reference). Classifiers*
286 *were built to predict one-vs-rest for that cancer type. BI = Broad Institute of MIT and Harvard;*
287 *BCM = Baylor College of Medicine; HMS = Harvard Medical School; MDA = MD Anderson*
288 *Institute for Applied Cancer Science; WUSTL = Washington University School of Medicine. (d)*
289 *Multinomial (mean) classification accuracy of classifiers to predict cancer type given the log-*
290 *ratios computed from the top and bottom 200 taxa associated with each cancer type. Random*
291 *Forests classifier, which is frequently used in this field but is not based on differential*
292 *abundance, was included as a comparison for this class of methods. Classifications were*
293 *performed within each center to remove batch effects from predictions. BIRDMAN outperforms*
294 *all other methods, including Random Forests, for all tumor types. (e) Clustermap of Kendall tau*
295 *correlation coefficients of pairwise cancer type differentials (breast cancer as reference). (f)*
296 *Comparison of lung-associated genera with GI-associated genera. Highlighted genera are*
297 *known to be associated with either lung or GI microbiome and show strong directionality in the*
298 *BIRDMAN results. (g) Venn diagram of genera present in TCGA lung samples and genera*
299 *present in advanced stage lung cancer from work published by Tsay et al. Additionally, the 22*
300 *genera represented in the top 100 features associated with TCGA lung cancer cancers are*
301 *included. A majority of these genera (16/22) are present in both datasets.*

302 Discussion

303 Advances in Bayesian computation have lowered the barriers to developing statistical
304 workflows. To empower microbiome scientists to take advantage of these methods, we
305 developed and implemented a novel approach to differential abundance based on Bayesian
306 hierarchical modeling, with advantages highlighted in simulation benchmarks and real-world
307 datasets. Chiefly, BIRDMAN is designed as a *framework* for researchers to account for the
308 statistical constraints specific to their biological questions. We have demonstrated the benefits
309 of this framework in common biological scenarios involving longitudinal study designs and
310 sequencing center variation — where BIRDMAN can better correct for technical variation than
311 existing methods while identifying biologically-relevant signals. In addition to the ability to
312 construct novel DA models, we presented a robust method for benchmarking and comparing
313 results from different DA tools. In contrast to previous efforts investigating FDR in simulation
314 and reproducibility benchmarks^{19,49,50}, we show how to construct sample classifiers from the log-
315 fold change estimates, enabling machine learning techniques such as cross-validation on
316 biological datasets.

317
318 Another key challenge of DA benchmarking is the absence of “ground truth,” or the true
319 differentials associated with biological conditions, especially in the presence of strong batch
320 effects. Simulations with known parameters for batch and biological effects can address this
321 limitation, and we showed that BIRDMAN models could recover, with high accuracy and

322 precision, these parameters and their uncertainty. Additional simulations on parameter
323 uncertainty further showed decreases with increased sample size and higher sequencing depth,
324 corroborating previous work and traditional statistical knowledge.

325
326 We then investigated two real-world case studies—antibiotics response/recovery and cancer
327 microbiome interactions—demonstrating how BIRDMan can uncover expected and novel
328 biology. For each dataset, BIRDMan models were able to account for the inherent effects of
329 center/subject on individual microbial abundances while, when necessary, accounting for
330 complex statistical factors (such as, random intercepts, random slopes, overdispersion). To
331 date, there is no other DA tool that provides a similar and necessary degree of flexible statistical
332 modeling. Our results on the previously published antibiotics dataset revealed the attenuating
333 effect of repeated Cp courses on Gram-negative bacteria, with potential implications for clinical
334 practice using antibiotics. Additionally, BIRDMan-informed results from the cancer microbiome
335 dataset could be useful in developing novel diagnostic and therapeutic strategies that target or
336 perturb cancer-specific features.

337
338 In light of our findings, there are notable assumptions that need to be considered. Specifically,
339 the choice of prior distributions affects the estimated posterior distributions, especially at low
340 sample sizes. Although priors allow researchers to include their expertise in their modeling
341 procedure, it is often the case that an appropriate prior distribution is unknown, requiring
342 uninformed priors with high uncertainty to be used. However, we note that as more analyses are
343 performed, their results can provide a rationale for picking future priors—a strong advantage of
344 the Bayesian approach over non-Bayesian methods. For our purposes, we defined the same
345 prior distribution for each feature within a dataset, but this can easily be adapted to better model
346 features with their expected parameter range. We also note that the (common) lack of absolute
347 abundance data is a limitation⁵¹ in evaluating differential abundance⁵¹. Strategies to account for
348 this, such as in Williamson *et al.*⁵², could potentially be translated into BIRDMan models to
349 augment the modeling results. Furthermore, we model the microbial abundances using the
350 negative binomial approach, which is currently contested as an appropriate model for
351 sequencing count data⁵³. Still, an advantage of BIRDMan is that the likelihood function is not
352 restricted to the negative binomial, and one can exchange it for the Poisson-Lognormal,
353 Multinomial, or any other count distribution⁵⁴.

354
355 To summarize, we find that careful statistical consideration during DA analysis enables the
356 identification of microbe-phenotype associations that are missed by existing tools. The flexibility
357 of BIRDMan can thoroughly account for unwanted confounding factors, such as batch and
358 subject, resulting in higher confidence in reported microbial biomarkers. Moreover, the
359 presented log-ratio benchmarking approach opens up numerous possibilities for testing
360 improved machine learning capabilities on microbiome data. Overall, we posit that BIRDMan's
361 flexibility and utility will provide impactful statistical results for complex study designs while
362 enabling reproducible science in the microbiome field.

363

364 Methods

365 Performing Bayesian inference with Stan

366 Parameter estimation was performed using Bayesian inference. Our approach utilizes Bayes' Rule where θ represents the parameter space and D represents our collected data:

$$P(\theta|D) = \frac{P(D|\theta)P(\theta)}{P(D)} .$$

369
370

371 Because the evidence term, $P(D)$, is simply a normalizing constant, we can rewrite Bayes' Rule
372 as follows, substituting terms with their common nomenclature:

373

$$\text{Posterior} \sim \text{Likelihood} \cdot \text{Prior}$$

374
375

376 Thus, our objective with Bayesian inference is to obtain the posterior distribution by modeling
377 the likelihood function of our data as well as our prior knowledge of the parameters. Absent a
378 model formulation involving conjugate priors, we cannot compute the posterior distribution
379 analytically. Instead, we use Stan to draw samples from the posterior distribution using the No-
380 U-Turn Hamiltonian Monte Carlo sampler²⁰. A series of Markov chains are initialized and
381 allowed to “warm-up” in their exploration of the parameter posterior distributions. Once the
382 defined number of warm-up iterations has concluded, a set number of samples are drawn from
383 each of the chains. Multiple chains are run to ensure that model convergence occurs.

384

385 We implement Bayesian inference using the CmdStanPy interface in Python, calling the C++
386 Stan toolchain for efficient sampling. The warm-up iterations are discarded by default and the
387 sampling iterations are saved for each Markov chain.

388 Negative binomial model parameterization

389 We fit counts of each microbe in a dataset according to a negative binomial distribution as an
390 approximation of multinomial logistic regression⁵⁵. Due to overdispersion, standard count
391 models such as Poisson are inappropriate for sequencing data²¹. We note that the negative
392 binomial model can be considered an extension to the Poisson model with additional variance
393 components⁵⁶.

394

395 The negative binomial models used in this work are described by parameters for both mean and
396 overdispersion. This is in contrast to traditional parameters in negative binomial models
397 described by the probability of success and the number of failures before an instance of a
398 success. The former model, often referred to as the “alternative parameterization,” is more
399 amenable to generalized linear modeling through hierarchical models as the mean can be
400 modeled directly.

401

402 The basic format of the alternative parameterization negative binomial model is described below
403 where n corresponds to the count, ϕ the overdispersion, and μ the mean count.

404

$$\text{NB}(n | \mu, \phi) = \binom{n + \phi - 1}{n} \left(\frac{\mu}{\mu + \phi} \right)^n \left(\frac{\phi}{\mu + \phi} \right)^\phi$$

405

406

407 We use a log-link function, $\mu = \exp(\eta)$ to model the mean where the log mean count, η , can be
408 represented by linear terms. To account for variable sequencing depth among samples, we
409 include log sequencing depth as an offset term in our models.

410 BIRDMAN framework

411 We developed BIRDMAN as a framework for highly-customizable Bayesian differential
412 abundance modeling. BIRDMAN abstracts much of the Bayesian workflow away for usage with
413 microbiome data. An object-oriented approach allows users to subclass basic models for their
414 custom implementations. BIRDMAN includes, by default, a Negative Binomial model
415 implementation. This can be used without writing any new Stan code or subclassing any
416 BIRDMAN objects.

417

418 BIRDMAN models take BIOM tables⁵⁷ as input containing the sample and observation IDs.
419 Sample metadata can be provided as Pandas DataFrames. We provide a method,
420 `create_regression`, with which users can provide an R-style formula to automatically create the
421 design matrix using the patsy Python package. Another method, `specify_model`, allows the
422 specification of the desired parameters and dimensions to return. This method is used by
423 `create_inference` to convert CmdStanPy output to ArviZ⁵⁸ InferenceData objects.

424

425 There are two base classes included with BIRDMAN termed the `TableModel` and the
426 `SingleFeatureModel`. The `TableModel` allows fitting an entire dataset at once, while the
427 `SingleFeatureModel` allows for fitting individual features. The `SingleFeatureModel` is
428 advantageous as it allows for highly parallelized workflows. Because there are often hundreds
429 or thousands of features in a microbiome dataset, we note that using multiple CPUs to run many
430 features at once is often more efficient than fitting the entire table. We provide a convenience
431 class, `ModelIterator`, to iterate through the features in a given table. This class also allows for
432 dividing the table into chunks. This allows users to customize the number of features to fit at
433 once depending on their computational resources.

434 Simulations

435 All simulations were performed through the `fixed_param` option in CmdStanPy. Ground-truth
436 parameters were provided into a negative binomial generative model to simulate data from
437 mean and dispersion parameters.

438

439 For the data-driven simulation, we randomly drew values for batch offset, batch dispersion, and
440 base dispersion parameters. These parameters were fed into a model with $\beta_0 = N(-8, 1)$,

441 $\beta_1 = N(2, 1)$. Log sampling depth was simulated from a Poisson-Lognormal distribution with λ
442 drawn from $N(5000, 0.2)$. We simulated 300 samples comprising 10 total batches with 10 total
443 features.

444
445 For the variable sample size simulations, we simulated feature counts for 500 samples with

446 $\beta_0 = 8$, $\beta_1 = 3$, and $\frac{1}{\phi} = 10$. Log sequencing depths were simulated using a Poisson-
447 Lognormal model with λ drawn from $N(50000, 0.5)$ where depth varied.

448
449 To simulate variable rarefaction depth, we first drew ground truth intercept and beta values from
450 $N(-8, 1)$ and $N(2, 1)$ respectively for 1000 features. These values were used to generate
451 counts for 300 samples through the multinomial distribution. We used the multinomial
452 distribution to enforce the same sampling depth for all samples, simulating rarefaction.

453 Antibiotics case study

454 16S data was downloaded from Qiita study 494; we used 16S OTUs picked against the
455 GreenGenes_13.8⁵⁹ reference database at 97% sequence similarity. OTU picking was
456 performed with SortMeRNA⁶⁰ with Qiita default parameter values. Features present in fewer
457 than 10 samples were filtered. We also removed samples with a total sequencing depth less
458 than 1000.

459
460 To account for the longitudinal nature of this design, we used backwards difference encoding
461 such that each time point was compared to the one immediately before it. We implemented the
462 subject identifiers as a random effect with both random intercepts and random slopes. The
463 posterior draws were centered around the mean. Ranking of OTUs by differentials for log-ratio
464 feature selection was done using the posterior means.

465
466 We performed t-tests comparing the log-ratios between groups of samples at different
467 timepoints. The alternative hypothesis was chosen such that samples from the later time point
468 would have higher log-ratios than those from the initial timepoint due to the anticipated effect of
469 Cp on microbial populations.

470
471 We then implemented multinomial logistic regression, random forest classification, and repeated
472 k-fold cross-validation through scikit-learn for our machine learning approach. Because DESeq2
473 supports contrasts natively, we computed the same contrasts as BIRDMAN for parity. With
474 ALDEx2 and ANCOM-BC, we computed the differentials associated with each timepoint using
475 preCp as reference. For the random forest classifier, we used the CLR-transformed feature
476 table (with a pseudocount of 1) entries as the predictors. All models were also provided one-hot-
477 encoded vectors for subject identifiers. Performance was measured using balanced accuracy.
478 For multinomial logistic regression we used the lbfgs solver with 1000 max iterations. For the
479 random forest classifier we used a set random seed and 100 estimators. We used repeated
480 stratified k-fold cross validation with 5 splits and 10 repeats and a random seed. All other
481 parameters not mentioned were set to the scikit-learn defaults.

482
483 Posterior draws for timepoint-contrast differentials were analyzed with (1) FirstCp-associated
484 features with preCp-associated features as reference and (2) SecondCp-associated features
485 with Interim-associated features as reference. In this way, the posterior distribution reflects how
486 each Cp course affects the selected bacterial features over time.

487
488 For determining the Gram status of each OTU, we used the BugBase⁶¹ web interface. We took
489 the set intersection of Gram positive and Gram negative features with the features associated
490 with both FirstCp and SecondCp to determine the Gram status breakdown of both numerator
491 and denominator features.

492 TCGA case study

493 The bacterial TCGA tables were obtained from those processed in Narunsky-Haziza et al.⁶² and
494 Poore et al.⁴ All TCGA sequence data were accessed via the Cancer Genomics Cloud⁶³ (CGC)
495 as sponsored by SevenBridges (<https://cgc.sbgenomics.com>) after obtaining data access from
496 the TCGA Data Access Committee through dbGaP (<https://dbgap.ncbi.nlm.nih.gov/aa/wga.cgi?page=login>). On Qiita⁶⁴, TCGA WGS host-depleted and
497 quality-controlled fastq files were used to generate a metagenomic table by direct genome
498 alignments based on Woltka v0.1.1⁶⁵ against the RefSeq⁶⁶ release 200 (built as of May 14,
499 2020). The resulting tables can be found on Qiita under study ID 13722, of which we filtered to
500 only analyze the bacteria and then were subsequently decontaminated through decontam⁶⁷
501 (<https://github.com/benjjneb/decontam>) (version 1.14.0) following the protocol described in
502 Poore et al.⁴

503
504
505 After initial table generation, we removed samples from data submitting centers with very few
506 samples. We also filtered our data to only include samples from white, African-American, and
507 Asian races. Additionally, we only included samples from patients who were alive at the time of
508 sample procurement and retained only one sample per subject. To filter out lowly prevalent
509 features, we removed features present in fewer than 50 total samples. To remove samples with
510 low sequencing depth, we set a threshold of 500 reads. Finally, we included only cancer types
511 with at least 20 instances in the dataset for statistical power.

512
513 We then built statistical models to model the differential associated with each cancer type.
514 Because TCGA did not include “normal” samples from healthy individuals, we used breast
515 cancer (BRCA) tumor samples as reference. Both race⁶⁸ and gender were also included as
516 covariates. Data submitting center was incorporated as a random effect (both random intercepts
517 and random slopes).

518
519 Posterior means were computed for each feature's association with each individual cancer type.
520 For each cancer type, we ranked the differentials and used the top and bottom 200 features
521 associated with that cancer type to compute log-ratios per sample. These log-ratios were used
522 as predictor variables in our machine learning models.

523

524 Because not every cancer type was represented in each center, we performed multi-class
525 classification within centers. For each center, we fit a model to predict cancer type from our log-
526 ratios. This procedure was performed with 5 repeats of stratified 2-fold cross-validation. We
527 repeated this machine learning process for cancer type differentials from DESeq2, ALDEx2, and
528 ANCOM-BC. For comparison, we fit a random forest classifier on the CLR-transformed feature
529 table to predict cancer type as well.

530
531 The leave-one-center-out models were fit using binomial logistic regression with balanced class
532 weights. For each cancer type, we fit a model on all but one center and used that model to
533 predict cancer type for the held-out center. We also used the same random forest classifier as
534 previously described for comparison.

535 Analysis & visualization software

536 Analysis of the results in this work were primarily performed through Python (v3.8.13). Pandas⁶⁹
537 (v1.1.5) and NumPy⁷⁰ (v1.22.3) were used for general data analysis. SciPy⁷¹ (v1.7.3) was used
538 for computing statistical tests. For interfacing with multidimensional arrays we used xarray⁷²
539 (v0.20.1) and ArviZ⁵⁸ (0.12.1). Machine learning models were fit and cross-validated using
540 scikit-learn⁷³ (v1.0.2). Python figures were generated using seaborn⁷⁴ (v0.11.2) and Matplotlib⁷⁵
541 (v3.5.1) as well as Matplotlib-venn (v0.11.7). We used biom-format⁵⁷ (2.1.12) and scikit-bio
542 (v0.5.6) for statistical analysis of microbiome data structures.

543
544 R analysis was performed using the tidyverse⁷⁶ packages dplyr (v1.0.9), stringr (v1.4.0), and
545 ggplot2 (v3.3.6). Phylogenetic visualization was performed using treeio⁷⁷ (v1.18.0) and ggtree⁷⁸
546 (v3.2.0). BIOM tables were read using the biomformat R package (v1.22.0).

547 Code and data availability

548 All data used were downloaded from publicly available Qiita studies. The scripts and Stan
549 models used to analyze these data as well as Jupyter notebooks for the visualizations are
550 available at <https://github.com/knightlab-analyses/birdman-analyses-final>. The BIRDMan
551 software package is available at <https://github.com/biocore/BIRDMan> and the documentation is
552 available at <https://birdman.readthedocs.io/>. All analyses in this work were performed using
553 BIRDMan v0.1.0.

554 Acknowledgments

555 We thank the members of the Knight Lab and Morton Lab for feedback and bug reporting for the
556 BIRDMan software. We thank the developers of ArviZ and CmdStanPy for responding to and
557 addressing issues on GitHub as well as the users on the Stan forums for answering our
558 questions.

559

560 This work was supported in part by NIH U19AG063744, NIH 1DP1AT010885, and NIH
561 U24CA248454. J.T.M. was funded by the intramural research program of the Eunice Kennedy
562 Shriver National Institute of Child Health and Human Development (NICHD).

563 Author information

564 G.R., J.T.M., and R.K. conceived the idea for the study. G.R. & J.T.M. developed the BIRDMAN
565 software package. G.R., J.T.M., C.G., G.D.S.-P., & C.M. contributed to the case study and
566 simulation analysis. C.A., J.T.M., C.M., & R.K. helped to define the scope of the analyses. G.R.
567 & Y.C. contributed to the documentation for BIRDMAN. M.E., Y.C., D.H., & C.M. gave critical
568 feedback on the usage and documentation of the software. All authors helped write and review
569 the manuscript.

570 Conflicts of interest

571 G.D.S.-P. and R.K. are inventors on a US patent application (PCT/US2019/059647) submitted
572 by The Regents of the University of California and licensed by Micronoma; that application
573 covers methods of diagnosing and treating cancer using multi-domain microbial biomarkers in
574 blood and cancer tissues. G.D.S.-P. and R.K. are founders of and report stock interest in
575 Micronoma. G.D.S.-P. has filed several additional US patent applications on cancer bacteriome
576 and mycobiome diagnostics that are owned by The Regents of the University of California or
577 Micronoma. R.K. additionally is a member of the scientific advisory board for GenCirq, holds an
578 equity interest in GenCirq, and can receive reimbursements for expenses up to US \$5,000 per
579 year.

580 References

- 581 1. Sochocka, M. *et al.* The Gut Microbiome Alterations and Inflammation-Driven Pathogenesis
582 of Alzheimer's Disease—a Critical Review. *Mol. Neurobiol.* **56**, 1841–1851 (2019).
- 583 2. Fouquier, J. *et al.* The Gut Microbiome in Autism: Study-Site Effects and Longitudinal
584 Analysis of Behavior Change. *mSystems* **6**, e00848-20 (2021).
- 585 3. Wirbel, J. *et al.* Meta-analysis of fecal metagenomes reveals global microbial signatures that
586 are specific for colorectal cancer. *Nat. Med.* **25**, 679–689 (2019).
- 587 4. Poore, G. D. *et al.* Microbiome analyses of blood and tissues suggest cancer diagnostic
588 approach. *Nature* **579**, 567–574 (2020).
- 589 5. Villapol, S. Gastrointestinal symptoms associated with COVID-19: impact on the gut

- 590 microbiome. *Transl. Res.* **226**, 57–69 (2020).
- 591 6. Zuo, T. *et al.* Alterations in Fecal Fungal Microbiome of Patients With COVID-19 During Time
592 of Hospitalization until Discharge. *Gastroenterology* **159**, 1302-1310.e5 (2020).
- 593 7. Poyet, M. *et al.* A library of human gut bacterial isolates paired with longitudinal multiomics
594 data enables mechanistic microbiome research. *Nat. Med.* **25**, 1442–1452 (2019).
- 595 8. Kostic, A. D. *et al.* The dynamics of the human infant gut microbiome in development and in
596 progression toward type 1 diabetes. *Cell Host Microbe* **17**, 260–273 (2015).
- 597 9. Proctor, L. M. *et al.* The Integrative Human Microbiome Project. *Nature* **569**, 641–648 (2019).
- 598 10. Gopalakrishnan, V. *et al.* Gut microbiome modulates response to anti-PD-1
599 immunotherapy in melanoma patients. *Science* **359**, 97–103 (2018).
- 600 11. Spencer, C. N. *et al.* Dietary fiber and probiotics influence the gut microbiome and
601 melanoma immunotherapy response. *Science* **374**, 1632–1640 (2021).
- 602 12. Lee, K. A. *et al.* Cross-cohort gut microbiome associations with immune checkpoint
603 inhibitor response in advanced melanoma. *Nat. Med.* **28**, 535–544 (2022).
- 604 13. Hiergeist, A., Reischl, U. & Gessner, A. Multicenter quality assessment of 16S ribosomal
605 DNA-sequencing for microbiome analyses reveals high inter-center variability. *Int. J. Med.*
606 *Microbiol.* **306**, 334–342 (2016).
- 607 14. Wang, Y. & LêCao, K.-A. Managing batch effects in microbiome data. *Brief. Bioinform.*
608 **21**, 1954–1970 (2020).
- 609 15. Chen, W. *et al.* A comparison of methods accounting for batch effects in differential
610 expression analysis of UMI count based single cell RNA sequencing. *Comput. Struct.*
611 *Biotechnol. J.* **18**, 861–873 (2020).
- 612 16. Vandeputte, D. *et al.* Quantitative microbiome profiling links gut community variation to
613 microbial load. *Nature* **551**, 507–511 (2017).
- 614 17. Kumar, M. S. *et al.* Analysis and correction of compositional bias in sparse sequencing
615 count data. *BMC Genomics* **19**, 799 (2018).

- 616 18. Nixon, M. P., Letourneau, J., David, L. A., Mukherjee, S. & Silverman, J. D. A Statistical
617 Analysis of Compositional Surveys. Preprint at <https://doi.org/10.48550/arXiv.2201.03616>
618 (2022).
- 619 19. Nearing, J. T. *et al.* *Microbiome differential abundance methods produce disturbingly*
620 *different results across 38 datasets*. 2021.05.10.443486
621 <https://www.biorxiv.org/content/10.1101/2021.05.10.443486v1> (2021)
622 doi:10.1101/2021.05.10.443486.
- 623 20. Hoffman, M. D. & Gelman, A. The No-U-Turn Sampler: Adaptively Setting Path Lengths
624 in Hamiltonian Monte Carlo. Preprint at <https://doi.org/10.48550/arXiv.1111.4246> (2011).
- 625 21. McMurdie, P. J. & Holmes, S. Waste Not, Want Not: Why Rarefying Microbiome Data Is
626 Inadmissible. *PLOS Comput. Biol.* **10**, e1003531 (2014).
- 627 22. Äijö, T., Müller, C. L. & Bonneau, R. Temporal probabilistic modeling of bacterial
628 compositions derived from 16S rRNA sequencing. *Bioinforma. Oxf. Engl.* **34**, 372–380
629 (2018).
- 630 23. Silverman, J. D., Durand, H. K., Bloom, R. J., Mukherjee, S. & David, L. A. Dynamic
631 linear models guide design and analysis of microbiota studies within artificial human guts.
632 *Microbiome* **6**, 202 (2018).
- 633 24. Joseph, T. A., Shenhav, L., Xavier, J. B., Halperin, E. & Pe'er, I. Compositional Lotka-
634 Volterra describes microbial dynamics in the simplex. *PLOS Comput. Biol.* **16**, e1007917
635 (2020).
- 636 25. Joseph, T. A., Pasarkar, A. P. & Pe'er, I. Efficient and Accurate Inference of Mixed
637 Microbial Population Trajectories from Longitudinal Count Data. *Cell Syst.* **10**, 463-469.e6
638 (2020).
- 639 26. Shenhav, L. *et al.* Modeling the temporal dynamics of the gut microbial community in
640 adults and infants. *PLOS Comput. Biol.* **15**, e1006960 (2019).
- 641 27. Dethlefsen, L. & Relman, D. A. Incomplete recovery and individualized responses of the

- 642 human distal gut microbiota to repeated antibiotic perturbation. *Proc. Natl. Acad. Sci.* **108**,
643 4554–4561 (2011).
- 644 28. Martino, C. *et al.* Context-aware dimensionality reduction deconvolutes gut microbial
645 community dynamics. *Nat. Biotechnol.* **39**, 165–168 (2021).
- 646 29. Gibbons, S. M. Keystone taxa indispensable for microbiome recovery. *Nat. Microbiol.* **5**,
647 1067–1068 (2020).
- 648 30. Chng, K. R. *et al.* Metagenome-wide association analysis identifies microbial
649 determinants of post-antibiotic ecological recovery in the gut. *Nat. Ecol. Evol.* **4**, 1256–1267
650 (2020).
- 651 31. Morton, J. T. *et al.* Establishing microbial composition measurement standards with
652 reference frames. *Nat. Commun.* **10**, 2719 (2019).
- 653 32. Fernandes, A. D. *et al.* Unifying the analysis of high-throughput sequencing datasets:
654 characterizing RNA-seq, 16S rRNA gene sequencing and selective growth experiments by
655 compositional data analysis. *Microbiome* **2**, 15 (2014).
- 656 33. Lin, H. & Peddada, S. D. Analysis of compositions of microbiomes with bias correction.
657 *Nat. Commun.* **11**, 3514 (2020).
- 658 34. Love, M. I., Huber, W. & Anders, S. Moderated estimation of fold change and dispersion
659 for RNA-seq data with DESeq2. *Genome Biol.* **15**, 550 (2014).
- 660 35. Oliphant, C. M. & Green, G. M. Quinolones: A Comprehensive Review. *Am. Fam.*
661 *Physician* **65**, 455–465 (2002).
- 662 36. Card, R. M. *et al.* Impact of Ciprofloxacin and Clindamycin Administration on Gram-
663 Negative Bacteria Isolated from Healthy Volunteers and Characterization of the Resistance
664 Genes They Harbor. *Antimicrob. Agents Chemother.* **59**, 4410–4416 (2015).
- 665 37. Peterson, C. T., Sharma, V., Elmén, L. & Peterson, S. N. Immune homeostasis,
666 dysbiosis and therapeutic modulation of the gut microbiota. *Clin. Exp. Immunol.* **179**, 363–
667 377 (2015).

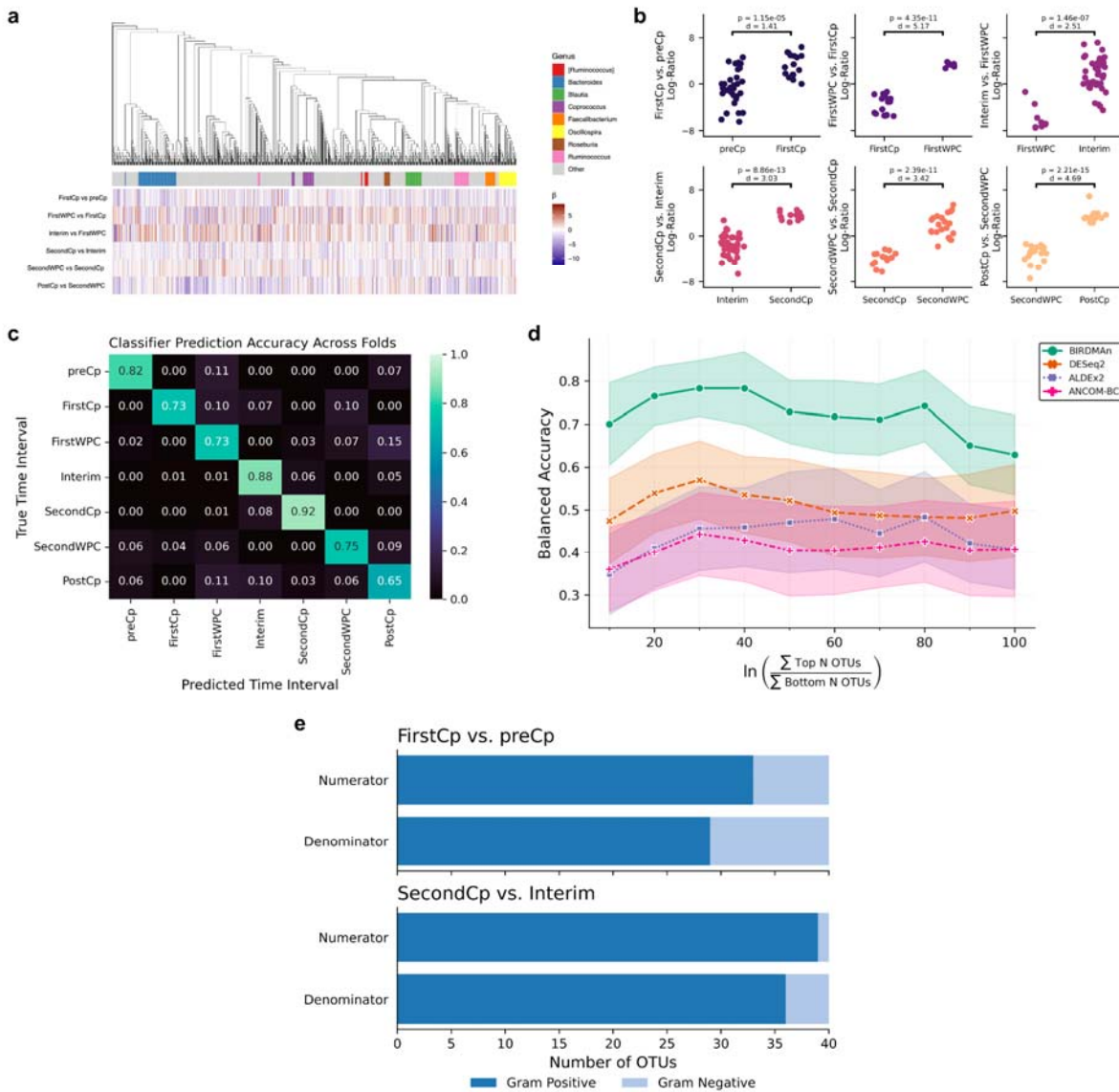
- 668 38. Ramirez, J. *et al.* Antibiotics as Major Disruptors of Gut Microbiota. *Front. Cell. Infect.*
669 *Microbiol.* **10**, (2020).
- 670 39. Weinstein, J. N. *et al.* The Cancer Genome Atlas Pan-Cancer analysis project. *Nat.*
671 *Genet.* **45**, 1113–1120 (2013).
- 672 40. Nejman, D. *et al.* The human tumor microbiome is composed of tumor type-specific
673 intracellular bacteria. *Science* **368**, 973–980 (2020).
- 674 41. Bullman, S. *et al.* Analysis of Fusobacterium persistence and antibiotic response in
675 colorectal cancer. *Science* **358**, 1443–1448 (2017).
- 676 42. Lo, C.-H. *et al.* Enrichment of *Prevotella intermedia* in human colorectal cancer and its
677 additive effects with *Fusobacterium nucleatum* on the malignant transformation of colorectal
678 adenomas. *J. Biomed. Sci.* **29**, 88 (2022).
- 679 43. Flemer, B. *et al.* Tumour-associated and non-tumour-associated microbiota in colorectal
680 cancer. *Gut* **66**, 633–643 (2017).
- 681 44. Nunley, D. R. *et al.* Allograft Colonization and Infections With *Pseudomonas* in Cystic
682 Fibrosis Lung Transplant Recipients. *Chest* **113**, 1235–1243 (1998).
- 683 45. Laroumagne, S. *et al.* Bronchial colonisation in patients with lung cancer: a prospective
684 study. *Eur. Respir. J.* **42**, 220–229 (2013).
- 685 46. Lambiase, A. *et al.* Sphingobacterium respiratory tract infection in patients with cystic
686 fibrosis. *BMC Res. Notes* **2**, 262 (2009).
- 687 47. Brumfield, K. D., Huq, A., Colwell, R. R., Olds, J. L. & Leddy, M. B. Microbial resolution
688 of whole genome shotgun and 16S amplicon metagenomic sequencing using publicly
689 available NEON data. *PLOS ONE* **15**, e0228899 (2020).
- 690 48. Durazzi, F. *et al.* Comparison between 16S rRNA and shotgun sequencing data for the
691 taxonomic characterization of the gut microbiota. *Sci. Rep.* **11**, 3030 (2021).
- 692 49. Hawinkel, S., Mattiello, F., Bijnens, L. & Thas, O. A broken promise: microbiome
693 differential abundance methods do not control the false discovery rate. *Brief. Bioinform.* **20**,

- 694 210–221 (2019).
- 695 50. Yang, L. & Chen, J. A comprehensive evaluation of microbial differential abundance
696 analysis methods: current status and potential solutions. *Microbiome* **10**, 130 (2022).
- 697 51. Gloor, G. B., Macklaim, J. M., Pawlowsky-Glahn, V. & Egozcue, J. J. Microbiome
698 Datasets Are Compositional: And This Is Not Optional. *Front. Microbiol.* **8**, (2017).
- 699 52. Williamson, B. D., Hughes, J. P. & Willis, A. D. A multiview model for relative and
700 absolute microbial abundances. *Biometrics* **78**, 1181–1194 (2022).
- 701 53. Hawinkel, S., Rayner, J. C. W., Bijmans, L. & Thas, O. Sequence count data are poorly fit
702 by the negative binomial distribution. *PLOS ONE* **15**, e0224909 (2020).
- 703 54. Townes, F. W. Review of Probability Distributions for Modeling Count Data.
704 *ArXiv200104343 Stat* (2020).
- 705 55. Taddy, M. Distributed multinomial regression. *Ann. Appl. Stat.* **9**, (2015).
- 706 56. Lindén, A. & Mäntyniemi, S. Using the negative binomial distribution to model
707 overdispersion in ecological count data. *Ecology* **92**, 1414–1421 (2011).
- 708 57. McDonald, D. *et al.* The Biological Observation Matrix (BIOM) format or: how I learned to
709 stop worrying and love the ome-ome. *GigaScience* **1**, 7 (2012).
- 710 58. Kumar, R., Carroll, C., Hartikainen, A. & Martin, O. ArviZ a unified library for exploratory
711 analysis of Bayesian models in Python. *J. Open Source Softw.* **4**, 1143 (2019).
- 712 59. McDonald, D. *et al.* An improved Greengenes taxonomy with explicit ranks for ecological
713 and evolutionary analyses of bacteria and archaea. *ISME J.* **6**, 610–618 (2012).
- 714 60. Kopylova, E., Noé, L. & Touzet, H. SortMeRNA: fast and accurate filtering of ribosomal
715 RNAs in metatranscriptomic data. *Bioinformatics* **28**, 3211–3217 (2012).
- 716 61. Ward, T. *et al.* BugBase predicts organism-level microbiome phenotypes. 133462
717 Preprint at <https://doi.org/10.1101/133462> (2017).
- 718 62. Narunsky-Haziza, L. *et al.* Pan-cancer analyses reveal cancer-type-specific fungal
719 ecologies and bacteriome interactions. *Cell* **185**, 3789–3806.e17 (2022).

- 720 63. Lau, J. W. *et al.* The Cancer Genomics Cloud: Collaborative, Reproducible, and
721 Democratized-A New Paradigm in Large-Scale Computational Research. *Cancer Res.* **77**,
722 e3–e6 (2017).
- 723 64. Gonzalez, A. *et al.* Qiita: rapid, web-enabled microbiome meta-analysis. *Nat. Methods*
724 **15**, 796–798 (2018).
- 725 65. Zhu, Q. *et al.* OGUes enable effective, phylogeny-aware analysis of even shallow
726 metagenome community structures. 2021.04.04.438427 Preprint at
727 <https://doi.org/10.1101/2021.04.04.438427> (2021).
- 728 66. Pruitt, K. D., Tatusova, T. & Maglott, D. R. NCBI reference sequences (RefSeq): a
729 curated non-redundant sequence database of genomes, transcripts and proteins. *Nucleic*
730 *Acids Res.* **35**, D61–D65 (2007).
- 731 67. Davis, N. M., Proctor, D. M., Holmes, S. P., Relman, D. A. & Callahan, B. J. Simple
732 statistical identification and removal of contaminant sequences in marker-gene and
733 metagenomics data. *Microbiome* **6**, 226 (2018).
- 734 68. Luo, M. *et al.* Race is a key determinant of the human intratumor microbiome. *Cancer*
735 *Cell* **40**, 901–902 (2022).
- 736 69. McKinney, W. Data Structures for Statistical Computing in Python. 6 (2010).
- 737 70. Harris, C. R. *et al.* Array programming with NumPy. *Nature* **585**, 357–362 (2020).
- 738 71. Virtanen, P. *et al.* SciPy 1.0: fundamental algorithms for scientific computing in Python.
739 *Nat. Methods* **17**, 261–272 (2020).
- 740 72. Hoyer, S. & Hamman, J. xarray: N-D labeled Arrays and Datasets in Python. *J. Open*
741 *Res. Softw.* **5**, 10 (2017).
- 742 73. Pedregosa, F. *et al.* Scikit-learn: Machine Learning in Python. *J. Mach. Learn. Res.* **12**,
743 2825–2830 (2011).
- 744 74. Waskom, M. L. seaborn: statistical data visualization. *J. Open Source Softw.* **6**, 3021
745 (2021).

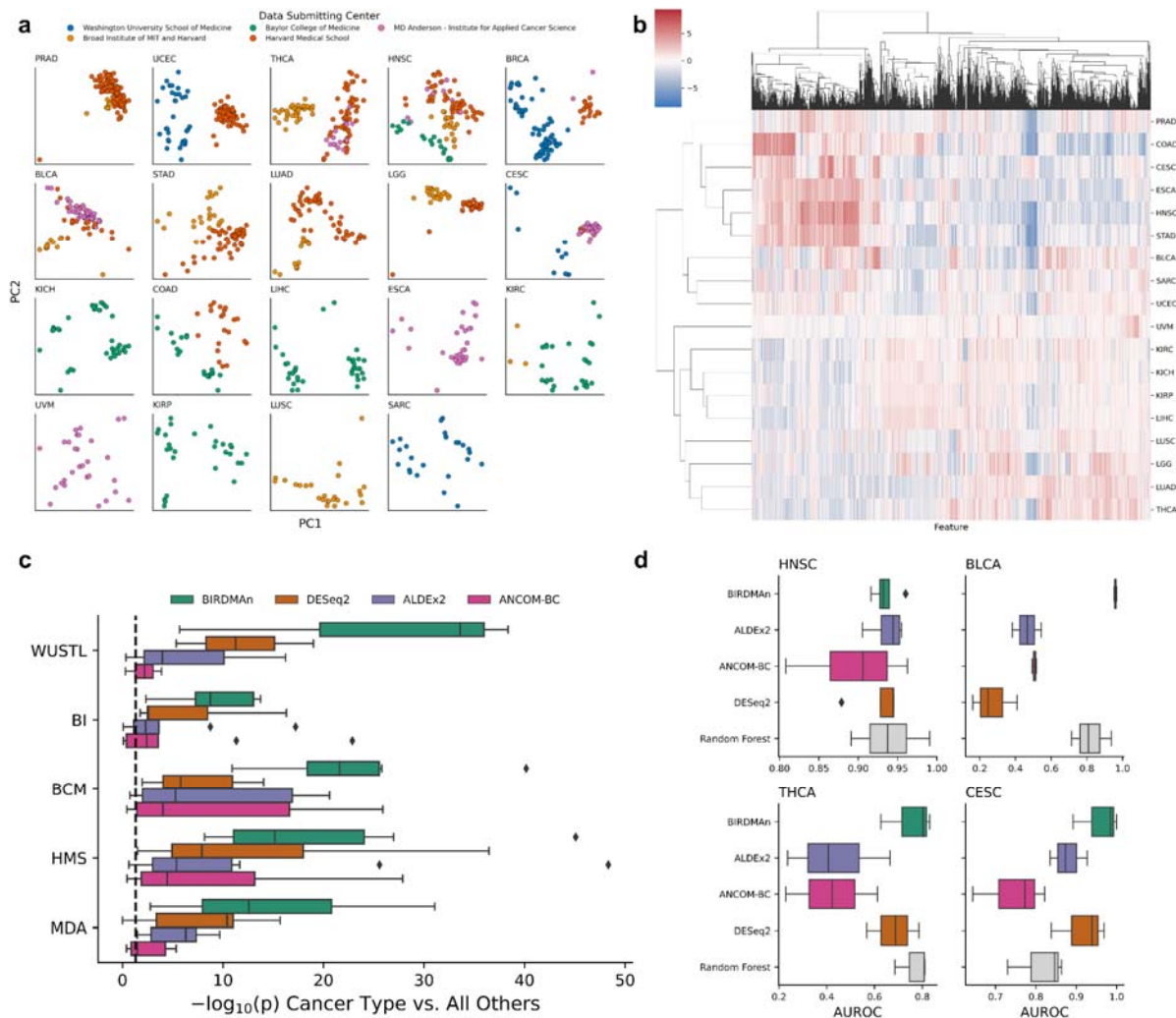
- 746 75. Hunter, J. D. Matplotlib: A 2D Graphics Environment. *Comput. Sci. Eng.* **9**, 90–95
747 (2007).
- 748 76. Wickham, H. *et al.* Welcome to the Tidyverse. *J. Open Source Softw.* **4**, 1686 (2019).
- 749 77. Wang, L.-G. *et al.* Treeio: An R Package for Phylogenetic Tree Input and Output with
750 Richly Annotated and Associated Data. *Mol. Biol. Evol.* **37**, 599–603 (2020).
- 751 78. Yu, G., Smith, D. K., Zhu, H., Guan, Y. & Lam, T. T.-Y. ggtree: an r package for
752 visualization and annotation of phylogenetic trees with their covariates and other associated
753 data. *Methods Ecol. Evol.* **8**, 28–36 (2017).

754 Supplementary Figures



755
 756 **Supplementary Fig 1:** (a) Phylogenetic tree of all OTUs with a heatmap of posterior means for
 757 each time-interval contrast. OTUs assigned to one of the top 8 most abundant genera are
 758 annotated through the colored strip. (b) When BIRDMAN is used to account for per-subject
 759 variation, log-ratio comparisons of the top 40 OTUs vs. bottom OTUs are associated with the
 760 difference between each time point and the next one. For each of these contrasts, the log-ratios
 761 of the samples between the two time intervals were compared using a one-sided t-test. Plots
 762 are annotated with p-values. Different taxa contribute to the log ratios for each contrast. (c)
 763 Overall performance of BIRDMAN classifier on predicting the antibiotics time interval using the
 764 log-ratios. The classifier prediction accuracies shown are aggregated across folds and repeats
 765 from repeated k-fold cross-validation. (d) Accuracy of the multinomial classifier by number of
 766 OTUs used in log-ratio calculations. Points represent mean accuracy across cross-validation

767 iterations and shaded areas represent ± 1 standard deviation. (e) Distribution of Gram positive
 768 and Gram negative OTUs associated with FirstCp and SecondCp log-ratios.
 769
 770



771
 772 **Supplementary Fig 2:** (a) RPCA projection of the original feature table subset to each
 773 individual cancer type. Points are colored by data submitting centers, showing that many cancer
 774 types exhibit strong separation by batch. (b) Posterior means (CLR) of feature differentials
 775 clustered by cancer type. (c) Log-ratios identified by BIRDMAN separate each tumor type from
 776 all others when stratified by center. Dashed line represents a t-test p-value at $p = 0.05$. (d)
 777 Performance of leave-one-center-out cross-validation logistic regression classifier AUROC of all
 778 methods.